Article

SPECT and PET Imaging of EGF Receptors with Site-Specifically Labeled EGF and Dimeric EGF

Zoya Levashova, Marina V. Backer, George Horng, Dean Felsher, Joseph M. Backer, and Francis G. Blankenberg

Bioconjugate Chem., **2009**, 20 (4), 742-749• DOI: 10.1021/bc800443w • Publication Date (Web): 25 March 2009

SPECT and PET Imaging of EGF Receptors with Site-Specifically Labeled EGF and Dimeric EGF

Zoya Levashova,[†] Marina V. Backer,[‡] George Horng,[§] Dean Felsher,[§] Joseph M. Backer,[‡] and Francis G. Blankenberg*,[†]

Department of Radiology/MIPS, Stanford University School of Medicine, Stanford, California 94305, Sibtech, Inc., Brookfield, Connecticut 06804, and Department of Medicine/Oncology, Stanford University School of Medicine, Stanford, California 94305.
Received October 15, 2008; Revised Manuscript Received February 25, 2009

We describe a new generation of tracers for molecular imaging of the cell surface receptors for epidermal growth factor (EGF). These receptors play a key role in the progression of many tumors and are major drug development targets. Our tracers are based on a recombinant human EGF expressed with a cysteine-containing tag that enables facile site-specific radiolabeling with ^{99m}Tc for single photon emission computed tomography or site-specific conjugation of ^{64}Cu PEGylated chelators for positron emission tomography. These tracers retain EGF activities *in vitro* and display selective and highly specific focal uptake in tumors *in vivo*. We expect that nuclear imaging of EGF receptors with these tracers will be useful for clinical diagnosis, therapeutic monitoring, and development of new drugs and treatment regimens.

INTRODUCTION

Tumor growth critically depends on growth factors, and epidermal growth factor (EGF) appears to be of particular significance for the progression of many tumors (*1*). EGF acts via transmembrane tyrosine kinase receptors (EGFR) and promotes cell proliferation, motility, and survival by activating STAT, MAPK, and PI3K/Akt pathways. Receptors for EGF are the major drug development targets, and several EGFR-directed therapeutics, including anti-EGFR antibodies and EGFR tyrosine kinase inhibitors, are entering the clinic. Currently, EGFR expression in individual patients is determined by immunohistochemical analysis of tumor biopsies. Clinical experience, however, revealed that only 10−25% of patients that are defined as EGFR-positive by immunohistochemical analysis respond to EGFR-directed therapeutics (*1*−*3*), and there is a poor correlation between EGFR immunohistochemistry and treatment outcome (*4*−*6*). Such poor predictive power is not particularly surprising because immunohistochemical analysis does not discriminate between active and inactive EGFR, while functional activity of the receptors appears to be critical for the prediction of response to EGFR-targeting therapeutics (*7*). Therefore, for more efficacious use of EGFR-targeting therapeutics, there is a need for information on EGFR activity in patients. In this respect, molecular imaging of functionally active EGFR could provide such information and might allow for (1) rational patient stratification, (2) rapid monitoring of responses to therapy, and (3) development of personalized treatment regimens.

Since ultimate proof of EGFR activity is binding and internalization of EGF, we consider EGF-based tracers the most suited for imaging of functionally active EGFR. To develop uniform EGF-based tracers, we have expressed EGF with an N-terminal Cys-tag, a 15-aa cysteine-containing fusion tag for site-specific conjugation of therapeutic and diagnostic payloads (*8*−*10*). Furthermore, since a functional EGF/EGFR complex contains two EGF molecules and two EGFR molecules, for this study we have also engineered a Cys-tagged dimeric EGF (dEGF) containing two genetically fused EGF moieties. We report here that EGF- and dEGF-based SPECT tracers can be prepared by direct radiolabeling of Cys-tag with ^{99m}Tc, while the corresponding PET tracers can be prepared by conjugating a PEGylated DOTA chelator to Cys-tag, followed by radiolabeling with ^{64}Cu. The favorable imaging and biodistribution characteristics of new EGF-based tracers, as well as the simplicity of their preparation, open the possibilities for further development.

EXPERIMENTAL PROCEDURES

Production of Cys-Tagged EGF and dEGF. The construction, expression, and purification of Cys-tagged EGF have been described recently (*8*). Briefly, EGF without a stop-codon was amplified by PCR from a DNA fragment encoding codon-optimized human EGF (kindly provided by Dr. P. T. Pienkos, Molecular Logix, Woodlands, TX), introducing NcoI sites to both termini of the PCR fragment, and cloned into an NcoI site of the pET/Hu-R4C(G_4S) vector for bacterial expression of proteins with Cys-tag (*10*). Clones with correct orientation of EGF were selected by colony PCR using T7-promoter-based sense and EGF-based antisense primers. The second copy of EGF including a stop-codon was cloned in-frame with the first EGF using the *Bam*HI site. The resulting plasmid encodes a 147-aa fusion protein comprising an N-terminal Cys-tag, a $(G_4S)_3$MG-linker, and EGF without a stop-codon connected to a second copy of EGF via a 9-aa linker SMAAIGSGF.

EGF and dEGF were refolded in red-ox buffer containing glutathione, and therefore, Cys-tag C4 thiol groups were protected in a mixed disulfide bond with glutathione in at least 90% of the protein. Prior to radiolabeling with ^{99m}Tc or conjugation of chelator, C4 thiol groups were deprotected by incubating the proteins with equimolar amounts of DTT at 25 °C for 20 min in 0.1 M Tris-HCl at pH 8.0 (*8*−*10*).

* Corresponding author. 725 Welch Road, Room #1673, Stanford, CA 94304-1601. Phone: 650-497-8601. Fax: 650-497-8745. E-mail: blankenb@stanford.edu.

[†] Department of Radiology/MIPS, Stanford University School of Medicine.

[‡] Sibtech, Inc.

[§] Department of Medicine/Oncology, Stanford University School of Medicine.

10.1021/bc800443w CCC: $40.75
Published on Web 03/25/2009

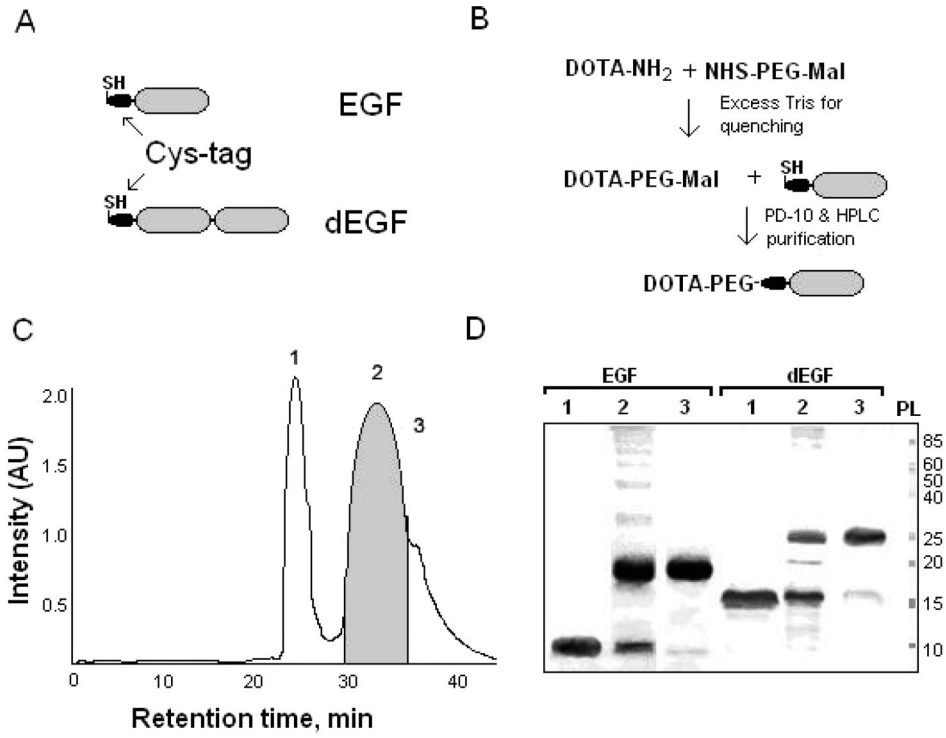

Figure 1. EGF and dEGF based conjugates. (A) Single or doubled copy of human EGF was cloned in-frame with the N-terminal Cys-tag (*9, 11*). Both proteins were expressed in *E.coli*, refolded into functionally active conformations in red-ox buffers, and purified via ion-exchange chromatography. (B) Flow chart of synthesis. (C) Separation of unmodified EGF (peak 1), EGF-PEG-DOTA (peak 2), and overmodified EGF-PEG-DOTA (peak 3) by RP-HPLC. Peak 2 (shown in gray) was collected, buffer-exchanged on a PD-10 column, and concentrated to 1−2 mg/mL. (D) Samples of unmodified EGF or dEGF (lanes 1), modification reaction mixtures (lanes 2), and RP-HPLC-purified products (lanes 3) were analyzed by reducing SDS−PAGE on 20% gels. PL, protein ladder (BioRad). Molecular weights are indicated in kDa.

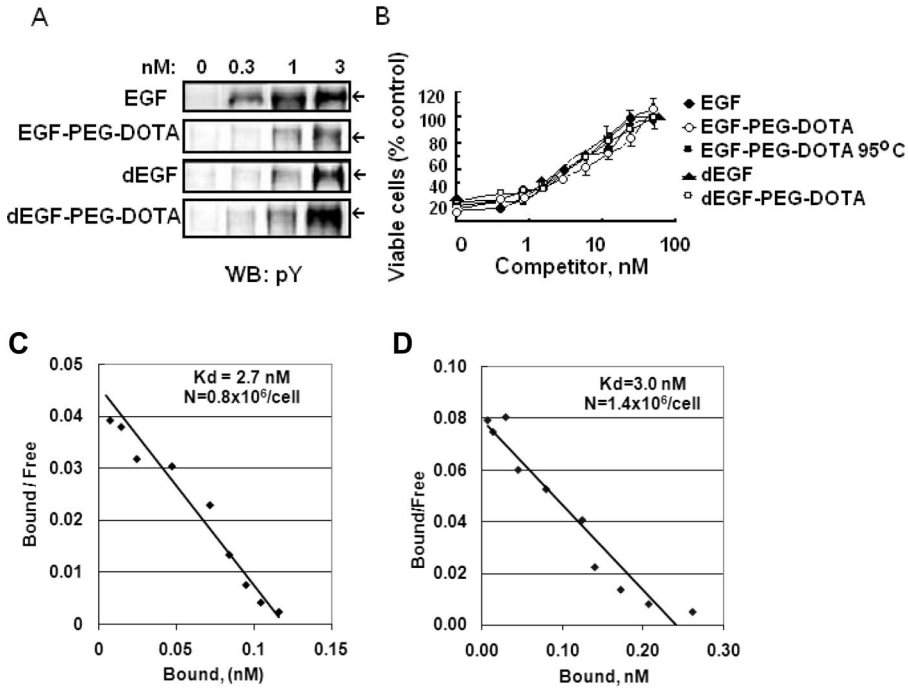

Figure 2. EGF- and dEGF-based conjugates are functionally active. (A) Induction of EGFR tyrosine autophosphorylation in rat F98/EGFR glioma cells. Arrows indicate positions of EGFR. 3.6×10^3 cell equivalents were loaded per one lane. (B) Competition with EGF-SLT fusion protein for binding to EGFR on human breast cancer cells MDA231luc. (C) Scatchard's analysis of EGF/Tc binding was undertaken with F98/EGFR cells. The values of K_d and N, the number of EGFR/cell, are indicated. (D) Scatchard's analysis of EGF-PEG-DOTA/Cu binding was undertaken with F98/EGFR cells. The values of K_d and N, the number of EGFR/cell, are indicated.

EGF and dEGF Direct Radiolabeling with ^{99m}Tc. Deprotected EGF or dEGF were radiolabeled, using a precursor complex [^{99m}Tc]-tricine, as described elsewhere for Cys-tagged single-chain VEGF (*9, 10*). Briefly, lyophilized tin-tricine reagent (a gift from Dr. J.-L. Vanderhyden, GE Healthcare, Piscataway, NJ) was reconstituted with 1.0 mL of degassed saline to give a final $SnCl_2 \cdot 2H_2O$ concentration of 0.6 mg/mL and a final tricine concentration of 20 mg/mL, pH 7.1. The

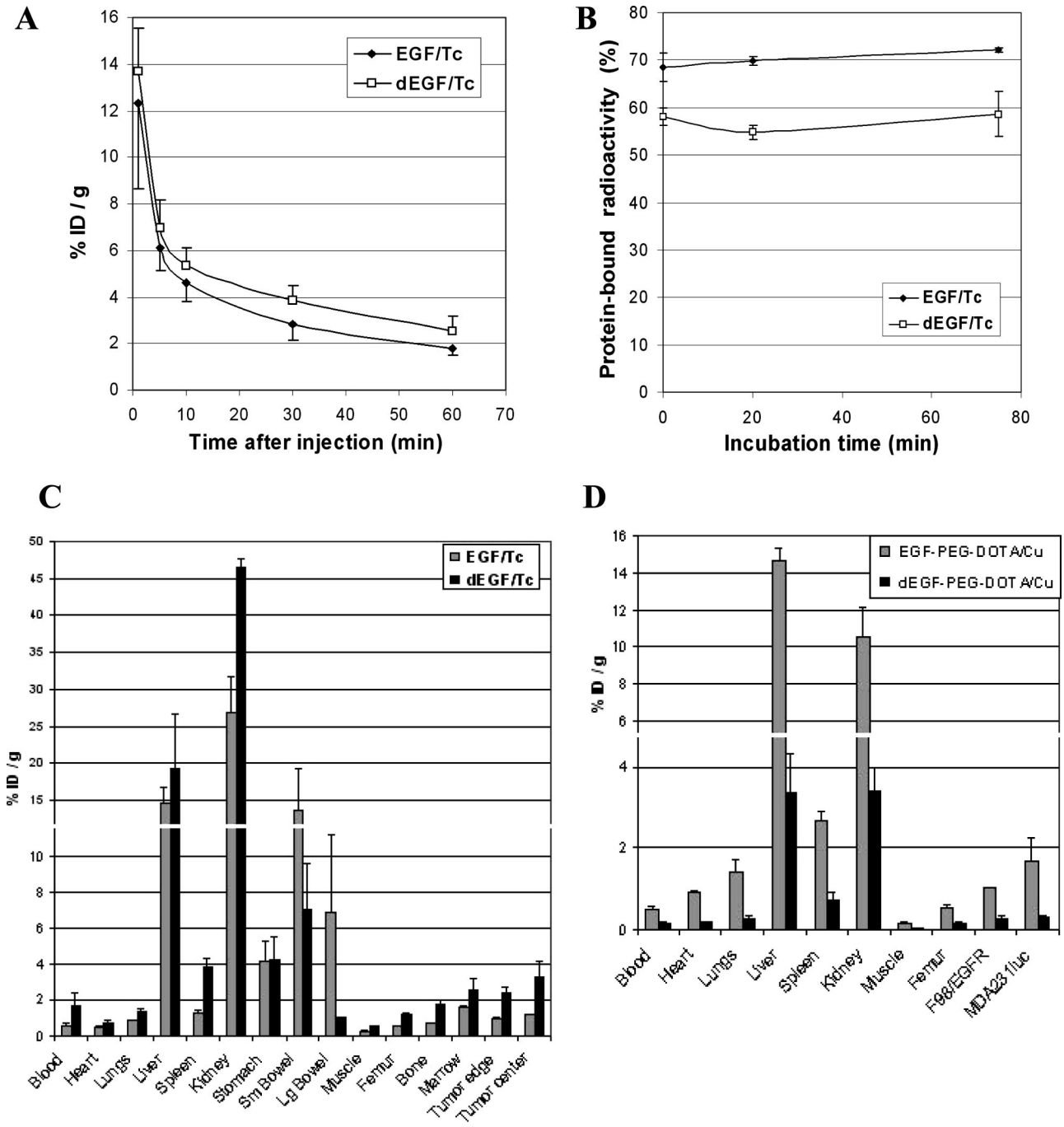

Figure 3. Tracer clearance, stability, and biodistribution. (A) Blood clearance of EGF/Tc and dEGF/Tc. (B) EGF/Tc and dEGF/Tc stability in murine plasma *ex vivo*. (C) Biodistribution of EGF/Tc (3.1 mCi/10 μg per mouse) and dEGF/Tc (0.81 mCi/13 μg per mouse) ($n = 4$ for every tracer) in 4 h after injection. (D) Biodistribution of EGF-PEG-DOTA/Cu (95 μCi/0.75 μg per mouse) and dEGF-PEG-DOTA/Cu (95 μCi/1.25 μg per mouse) in 22 h after injection ($n = 4$ for every tracer). Data for major organs are averaged for all tumor-bearing mice. Tumor uptake is averaged for specific tumors.

Table 1. Major Organ Uptake (%ID/g) for EGF-Based ^{99m}Tc Tracers

	EGF/Tc 3 h	dEGF/Tc 3 h	EGF-HYNIC/Tc/EDDA 4 h (*14*)	EGF-HYNIC/Tc 3 h (*13*)
kidney	27.0 ± 4.8	45.5 ± 1.4	96.3 ± 45.4	28.9 ± 14.0
liver	14.6 ± 2.3	24.5 ± 7.4	32.6 ± 13.2	29.2 ± 7.6

reaction mixture containing 10.0 μL of tin-tricine, 34 μg of deprotected protein, and 10 mCi of ^{99m}Tc-pertechnetate in a final volume of 50−100 μL was incubated for 30 min at 37 °C. Radiolabeled proteins, named EGF/Tc or dEGF/Tc, were purified by size-exclusion on PD-10 columns (GE Healthcare, Piscataway, NJ) equilibrated with phosphate-buffered saline (PBS). Specific activities ranged from 130 to 280 μCi/μg protein. The average purity before PD-10 purification was 45 ± 13% ($n = 13$), as judged by the amount of ^{99m}Tc eluted from PD-10 after the protein peak. Radiopurity after PD-10 was determined by ITLC using PBS as a solvent. We observed ^{99m}Tc batch-dependent variations of radiopurity in the range of 90−95%. The impurities migrated with the solvent front and appeared to arise from small and variable amounts of colloidal forms of ^{99m}Tc that were coeluted with radiolabeled protein from the PD-10 column but yielded migrating ^{99m}Tc under TLC conditions.

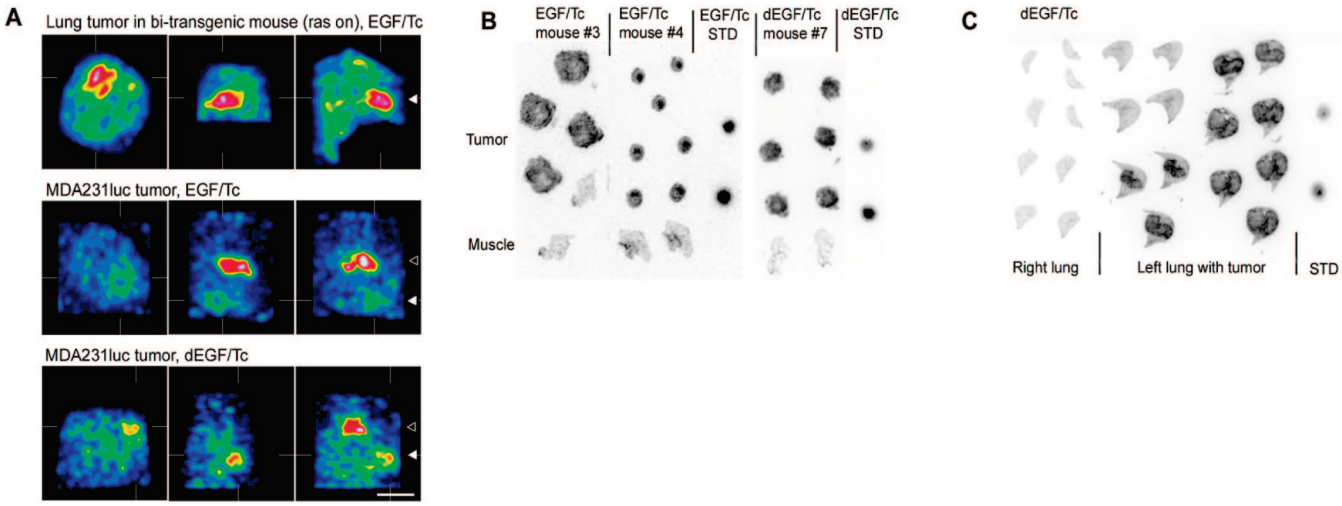

Figure 4. SPECT imaging and autoradiography. (A) SPECT images of mice injected with 3.1 mCi/10 μg of EGF/Tc or 1.7 mCi/13 μg dEGF/Tc per mouse. Representative transverse, sagittal, and frontal images are shown. Upper row: spontaneous lung tumor in bitransgenic mouse with ras-oncogene expression, EGF/Tc tracer. Middle row: orthotopic MDA231luc tumor, EGF/Tc tracer. Lower row: orthotopic MDA231luc tumor, dEGF/Tc tracer. The largest lung tumor and MDA231luc tumors are shown by white arrowheads. Open arrowheads show submandibular glands with nonspecific tracer uptake. The scale bar is 10 mm. (B) Autoradiographs of orthotopic MDA231luc tumors (25 days after cell injection). 3.1 mCi/10 μg per mouse of EGF/Tc or 1.7 mCi/13 μg of dEGF/Tc has been i.v. injected. STD is two spots of radioactivity equal 0.0016 and 0.0032% of injected dose. (C) Right (healthy) and left (tumor-invaded) lungs of a myc-on bitransgenic mouse injected with 4.5 mCi/20 μg of dEGF/Tc. STD is two spots of radioactivity equal to 0.0007 and 0.0014% of ID.

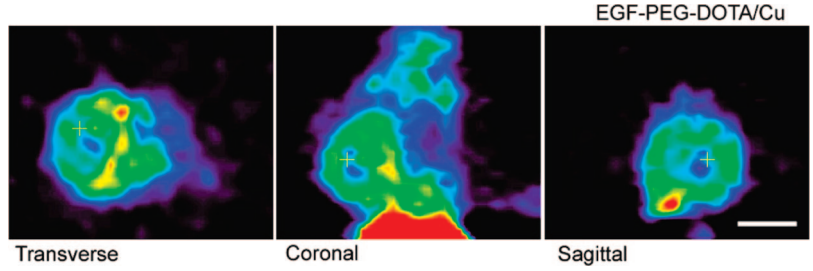

Figure 5. PET imaging. PET imaging of MDA231luc tumor (36 days after implantation). Representative transverse, coronal, and sagittal tomographic slices through the left mouse mammary fat pad tumor taken 3 h after an injection of 300 μCi of EGF-PEG-DOTA/^{64}Cu. The scale bar is 10 mm.

Radiolabeling of protected EGF and dEGF yielded ~20-fold less radioactivity in collected protein peaks, as compared with deprotected proteins. This low-level labeling is most likely due to the small amount of nonprotected C4 thiol groups generally present in preparations of Cys-tagged proteins.

Conjugation of DOTA to EGF or dEGF. DOTA was conjugated to EGF and to dEGF through a two-step procedure described elsewhere (*8, 10*), with minor modifications. Briefly, in step 1, functionalized DOTA was prepared by derivatization of *p*-NH_2-Bn-DOTA (2-(4-aminobenzyl)-1,4,7,10-tetraazacyclododecane-1,4,7,10-tetraacetic acid) (Macrocyclics, Dallas, TX) with 5 kDa of NHS-PEG-Mal, polyethylenglycol (PEG) containing an amino-reactive NHS group on the one end and a thiol-reactive maleimide on the other end of each PEG molecule (NOF America, Terrytown, NY). The reaction was performed at 2:1 DOTA to PEG molar ratio in a buffer containing 15 mM NaOAc, 50 mM Na_2CO_3, and 115 mM NaCl, pH 8.0. The reaction was incubated for 1 h at room temperature. Residual NHS was hydrolyzed by the addition of 1 M Tris HCl at pH 8.0 to a final concentration of 100 mM and incubated for 30 min. Functionalized DOTA-PEG-Mal was stored at −70 °C in small aliquots.

In step 2, the DOTA-PEG-Mal conjugate was added to freshly prepared deprotected protein at 2:1 maleimide to protein ratio and incubated for 1 h at room temperature. The reaction mixture was passed through PD-10 and then fractionated by RP-HPLC on a C4 column, which provided for a good separation of unmodified and PEGylated proteins. RP-HPLC purification was followed by solvent exchange on PD-10 to a buffer containing 0.1 M NaOAc at pH 5.5 and concentration of purified conjugates via reverse dialysis using Aquacide III powder (Calbiochem, San Diego, CA). Final preparations of EGF-PEG-DOTA and dEGF-PEG-DOTA were stored at °70 °C in small aliquots.

Radiolabeling of EGF-PEG-DOTA and dEGF-PEG-DOTA with ^{64}Cu. Conjugates were radiolabeled with ^{64}Cu, using a procedure developed previously for scVEGF-PEG-DOTA (*8, 10*). In a typical radiolabeling reaction, 20 μg of EGF-PEG-DOTA or dEGF-PEG-DOTA conjugate were mixed with 3.0−3.8 mCi of ^{64}Cu (Washington University Medical School, Saint Louis, MO) in 0.1 M NaOAc at pH 5.3−5.5 in the presence of DMSO (20% for EGF-PEG-DOTA and 30% for dEGF-PEG-DOTA) and incubated for 1 h at 55^o C. Residual free ^{64}Cu was sequestered by 1 mM EDTA. The reaction mixtures were passed through NAP-5 gel-filtration columns (GE Healthcare, Piscataway, NJ), yielding tracers with a specific activity of ~125 μCi/μg, for EGF-PEG-DOTA, and ~75 μCi/μg, for dEGF-PEG-DOTA.

Tissue Culture. F98/EGFR(F) rat glioma cells engineered to overexpress human EGFR were a kind gift from Dr. R. Barth (The Ohio State University, Columbus, OH). The high level of EGFR in these cells was supported by Scatchard analysis of radioligand binding, as described in the Results section. F98/EGFR(F) cells were grown in a 1:1 mixture of DMEM and F-12 nutrient mixture (Invitrogen, Carlsbad, CA), 5% FBS, and

2 mM L-glutamine. For prolonged cultivation, cells were maintained in 0.5 mg/mL of G418. For tumor implantation, cells were grown for 2−3 passages in complete medium without G418. MDA231luc cells expressing firefly luciferase were developed as described (*8*) from MDA-MB-231 mammary gland adenocarcinoma cells (ATCC # HTB-26) expressing a moderate level of EGFR, an average of 2×10^5 EGFR per cell (*11*). Approximately 5-fold difference in EGFR expression in MDA231luc and F98/EGFR(F) cells was supported by Western blot analysis of EGFR in cell lysates (data not shown). MDA231luc were cultured in high glucose DMEM (Invitrogen, Carlsbad, CA), 10% heat inactivated fetal bovine serum (FBS, HyClone, Logan, UT), and 2 mM L-glutamine. All cells were maintained at 37 °C and 5% CO_2.

Animals and Tumor Models. SCID mice (male, 5−6 week old) were purchased from Charles River Laboratories (Wilmington, MA). MDA231luc human breast carcinoma cells (*8, 9*) were implanted into the left axillary fat pad at 10^6 cells per mouse. F98/EGFR(F) rat glioma cells were implanted subcutaneously onto the right shoulder at 4.5×10^6 cells per mouse. The generation of spontaneous mouse lung adenocarcinomas in bitransgenic mice (FVBN original strain carrying *myc* or *ras* transgenes regulated by a tetracycline-inducible lung-specific promoter) has been described previously (*12*). The protocol for the animal studies was approved by the Stanford University Institutional Animal Care and Use Committee.

Stimulation of EGFR Phosphorylation in F98/EGFR(F) Cells. The EGFR tyrosine phosphorylation assay was performed as reported elsewhere (*8*). Briefly, near-confluent F98/EGFR(F) cells grown in 24-well plates were incubated overnight in serum-free DMEM, then shifted to serum-free DMEM with 0.5 mM sodium vanadate for 15 min at 37 °C. To stimulate EGFR tyrosine phosphorylation, proteins were added to cells to final concentrations in the range from 0 to 50 nM. After 10-min stimulation at 37 °C, cells were lyzed, separated by SDS−PAGE, and analyzed by Western blotting using phosphotyrosine-specific antibody PY clone PT-66 (Sigma, St Louis, MO). In these experiments, 3.6×10^3 cell equivalents were loaded per one lane.

Competition with EGF-SLT Fusion Cytotoxin for Binding to Cellular EGFR in MDA231luc Cells. MDA231luc cells were plated on 96-well plates 20 h before the experiment (1000 cells/well). Proteins were serially diluted in complete culture medium supplemented with EGF-SLT fusion cytotoxin (SibTech, Brookfield, CT) and added to cells in triplicate wells to a final EGF-SLT concentration of 1 nM and competitors ranging from 0 to 25 nM. EGF-SLT is highly toxic for MDA-231luc cells (IC_{50} of 50 pM); therefore, the ability of proteins to compete with EGF-SLT for binding to cellular EGFR can be readily measured by the numbers of surviving cells after a 72-h exposure. Viable cells were quantitated by CellTiter 96 AQ_{ueous} One Solution Cell Proliferation Assay kit (Promega, Madison, WI).

Scatchard's Analysis of Tracer Binding to Cellular EGFR. F98/EGFR(F) cells grown on 12-well plates were shifted to serum-free medium at room temperature for 45 min. Varying amounts of EGF/Tc or EGF-PEG-DOTA/Cu were added to cells in triplicate wells for 90 min, followed by two PBS and one high-salt (0.5 M NaCl in PBS) wash. Cells were lyzed in PBS containing 1% Triton X-100 and assayed for ^{99m}Tc or ^{64}Cu activity in a gamma counter (140 and 511 keV level, respectively, 20% window). Nonspecific binding was determined for the same amounts of labeled EGF supplemented with a 200-fold molar excess of cold EGF.

Stability of EGF/Tc and dEGF/Tc. For *in vivo* stability testing, Balb/c mice ($n = 2$) were injected via the tail vein with EGF/Tc (60 μCi/0.25 μg per mouse) or with dEGF/Tc (60 uCi/0.22 μg) and sacrificed 2 min later. Blood was collected and clarified by centrifugation. Plasma samples were incubated at 37 °C for 10, 20, and 75 min. Rough estimation of protein-bound radioactivity in 1-μL plasma aliquots was done by ITLC. Stability was also tested *in vitro* by incubating the tracers in PBS at room temperature followed by ITLC and SDS−PAGE analyses.

Blood Clearance and Biodistribution Studies. For blood clearance and biodistribution studies, tracers were injected via the tail vein, and serial ~50-μL blood samples were taken via the supraorbital sinus at various time points after injection. Tissue samples taken at specified time points were counted in a gamma counter along with three samples of standard activity (1/100 of injected dose). Results were calculated as the average of the percentage of injected dose (ID) or %ID per gram (g) of tissue ± one standard deviation of the mean.

SPECT Imaging and Autoradiography. For SPECT imaging, 1.7−4.5 mCi of tracer per mouse ($n = 4$) was injected via the tail vein. SPECT images were obtained 1 h after injection with the following parameters: 360° rotation, 64 steps, 30 s per step, 0.5 mm pinhole aperture, a 64 × 64 image matrix, and a 3.4 cm FOV using a small animal SPECT imaging gamma camera (A-SPECT, LumaGEM, Gamma Medica, Los Angeles). For autoradiography, tumors and pectoralis muscle from the healthy chest side were snap-frozen immediately after imaging, cryosectioned (60-μm thickness), and exposed to a phosphor storage screen for 16 h. For autoradiography of lung tumors, before freezing lungs have been perfused with 1% PFA in PBS followed by 20% sucrose in PBS. The phosphor screen images were read out with a laser digitizer at a resolution of 50 μm per pixel. Region of interest (ROI) analysis of radiotracer activity was performed using ImageQuant TL Software. The maximal cts/pixel of the rim and the average cts/pixel of the center of the tumor were normalized to corresponding contralateral pectoral muscle uptake (minimum cts/pixel).

PET Imaging. Two groups of tumor-bearing mice ($n = 8$) intravenously received 95 μCi of EGF-PEG-DOTA/Cu or dEGF-PEG-DOTA/Cu. Ten-minute static scans of mice in prone position were obtained on a microPET R4 rodent model scanner (Concorde Microsystems, Knoxville, TN) equipped with computer-controlled vertical and horizontal bed motion, with an effective axial field of view (FOV) of 7.8 cm and a transaxial FOV of 10 cm. Mice anesthetized with 2% isoflurane were placed near the center of the FOV to ensure the highest image resolution and sensitivity. The images were reconstructed by a two-dimensional ordered-subsets expectation maximum algorithm. No correction was necessary for attenuation and scattering. We obtained relative tumor or organ radioactivity concentrations from mean pixel values within the multiple ROI volumes. For biodistribution, tissue samples were taken at 22 h after injection and counted in a gamma counter along with three samples of standard activity (1/100 of injected dose). Results were calculated as the average of the percentage of injected dose per gram (%ID /g) of tissue ± one standard deviation of the mean.

RESULTS

Cys-Tagged EGF and dEGF and Site-Specific Conjugation of PEGylated DOTA Chelator. To make tracers for imaging EGF receptors, we used a previously described Cys-tagged EGF (*8*) and a newly engineered Cys-tagged head-to-tail EGF dimer (dEGF) (Figure 1A). We reasoned that since functional ligand/receptor complexes include two EGF molecules, dEGF might provide certain advantages in binding and/or internalization of tracers. EGF and dEGF were expressed in *E.coli*, recovered from inclusion bodies, refolded in red-ox buffer containing glutathione, and purified via ion-exchange chromatography (*8*). As

other Cys-tagged proteins refolded in red-ox buffer, EGF and dEGF proteins were recovered with the C4-thiol group in Cys-tag protected in a form of a mixed disulfide with glutathione. For direct radiolabeling with ^{99m}Tc or for conjugation of the DOTA chelator, the C4-thiol group was readily deprotected upon incubation with equimolar amounts of DTT.

The DOTA chelator was conjugated to the C4-thiol group in EGF or dEGF via a 5 kDa NHS-PEG-Mal linker, using a previously developed (*8*) two-step procedure (Figure 1B). First, NHS chemistry was used for conjugation of NHS-PEG-Mal to *p*-NH_2-Bn-DOTA, followed by quenching of unreacted NHS with excess of Tris HCl at pH 8.0. At the next step, the quenched reaction mixture, without further purification, was added to deprotected EGF or dEGF, and the resulting EGF-PEG-DOTA or dEGF-PEG-DOTA were purified by RP HPLC (Figure 1C). A typical preparation of RP HPLC purified EGF-PEG-DOTA or dEGF-PEG-DOTA contains less than 10% of unmodified or overmodified starting protein (Figure 1D).

Functional Activities of Proteins and Conjugates. Functional activities of EGF, dEGF, and the corresponding conjugates were tested in several cell-based assays. In a short-term assay (10 min), conjugates were tested for the ability to bind to EGFR and induce its tyrosine autophosphorylation. In this assay, both proteins and their conjugates displayed dose-dependent activities in a similar range (Figure 2A). Interestingly, EGF-PEG-DOTA was less active than EGF, while dEGF-PEG-DOTA was more active than dEGF. The latter data suggested that the presence of two PEG-DOTA moieties in the functional (EGF-PEG-DOTA)$_2$/EGFR$_2$ complex might be somewhat more detrimental for receptor binding than a single PEG-DOTA in the dEGF-PEG-DOTA/EGFR$_2$ complex.

In a long-term competition assay (3 days), conjugates were tested for their ability to protect EGFR-positive cells from EGF-SLT, a fusion cytotoxin, combining EGF and catalytic subunit A of Shiga-like toxin (Backer et al., submitted for publication). We reasoned that in this assay binding of EGF-based constructs to EGFR reaches equilibrium and therefore eliminates any kinetic effects that might affect short-term assays. We found that in this assay both parental proteins and corresponding EGF-PEG-DOTA and dEGF-PEG-DOTA displayed very similar activities (Figure 2B).

Since loading of the DOTA chelator with radionuclides takes place at elevated temperature, we also tested if such treatment would affect EGF activity. We found that incubation of EGF-PEG-DOTA conjugates in radiolabeling buffer at 95 °C for 30 min did not decrease its functional activity in the protection assay (Figure 2B).

Radiolabeling of Cys-Tagged EGF and dEGF with ^{99m}Tc. We have recently reported that Cys-tag in scVEGF can be directly radiolabeled with ^{99m}Tc using tin-tricine as a precursor complex and hypothesized that a similar radiolabeling can be undertaken with any Cys-tagged protein (*9*). Indeed, we found that deprotected EGF and dEGF, but not parental protected molecules, were readily radiolabeled with [^{99m}Tc]pertechnetate. After purification via size-exclusion chromatography on PD-10, we obtained EGF/Tc and dEGF/Tc tracers with specific activity in the range of 160−300 and 130−280 μCi/μg, respectively, and radiopurity in the range of 90−95%. The specific activity obtained through direct radiolabeling was compared favorably to the reported values 15−30 μCi/μg (*13*) or 82 μCi/μg (*14*) obtained after radiolabeling of the EGF-HYNIC conjugates with tin-tricin as a coligand, and 68 μCi/μg for EGF-HYNIC conjugates with EDDA as a coligand (*14*). As judged by a Scatchard analysis of EGF/Tc binding to F98/EGFR(F) cells, the procedure resulted in tracers with the expected low nanomolar affinity to EGFR (K_d = 2.7 nM) and indicated the presence of 0.8 × 10^6 EGFR/cell (Figure 2C). Notably, site-specifically radiolabeled EGF/Tc displayed 2−3-fold higher affinity to EGFR than that reported for EGF-HYNIC-Tc tracers obtained by random conjugation of the chelator, despite the fact that only one HYNIC molecule was conjugated per one EGF protein (*13*).

Radiolabeling of EGF- and dEGF-PEG-DOTA Conjugates with ^{64}Cu. The ^{64}Cu radiolabeling protocol was initially developed for scVEGF-PEG-DOTA conjugates (*8, 10*). As applied to EGF-PEG-DOTA and dEGF-PEG-DOTA, this procedure routinely resulted in a specific activity of ∼125 μCi/μg for EGF-PEG-DOTA and of ∼75 μCi/μg for dEGF-PEG-DOTA. As judged by Scatchard's analysis of binding of EGF-PEG-DOTA/Cu to F98/EGFR cells (Figure 2D), the K_d value of 3 nM and 1.4 × 10^6 of EGFR/cell for this tracer were close to that for the EGF/Tc tracer (see Figure 2C).

Stability, Blood Clearance, and Biodistribution Studies. ^{99m}Tc and ^{64}Cu radiolabeled tracers cleared rapidly from the circulation, with more than 95% of tracer cleared within 1 h after intravenous injection (Figure 3A for EGF/Tc). We found that these tracers are stable for at least 3 h at room temperature in PBS (not shown) and that radionuclides were protein-associated for at least 75 min at 37 °C in plasma (Figure 3B).

Biodistribution experiments with EGF/Tc and dEGF/Tc were performed on MDA231luc tumor-bearing mice (n = 4) with well-formed tumors at 25-day post implantation. At 3 h after intravenous injection, we found that uptake of dEGF/Tc in most organs, including tumors, was higher than that of EGF/Tc (Figure 3C). Interestingly, for both tracers, uptake at the edge of the tumor was very similar to uptake in the central tumor areas, suggesting that tracers are distributed throughout the tumor mass (Figure 3C). As summarized in Table 1, kidney uptake of EGF/Tc was ∼3-fold lower than that of EGF-HYNIC/Tc with EDDA as coligand (*14*), and comparable to that of EGF-HYNIC/Tc (*13*) with tricin as coligand. However, liver uptake of EGF/Tc was 2-fold lower than that for both EGF-HYNIC/Tc tracers (Table 1).

For biodistribution studies with EGF-PEG-DOTA/Cu and dEGF-PEG-DOTA/Cu, 95 μCi of either tracer were intravenously injected into mice (n = 4) 9 days after either MDA231luc or F98/EGFR tumor cell implantation, when tumors were just palpable (3−5 mm in diameter). We found that 22 h postinjection uptake of EGF-PEG-DOTA/Cu in all organs, including tumors, was ∼3-fold higher than that of dEGF-PEG-DOTA/Cu (Figure 3D). Interestingly, the uptake of both tracers in F98/EGFR(F) tumors was somewhat lower than in MDA231luc, despite the fact that the latter cells express ∼5-fold less EGFR in tissue culture (data not shown). We found this result very instructive since it indicated that only functional in vivo tests could provide meaningful information on the receptor activity *in vivo*.

SPECT Imaging and Autoradiographic Studies. SPECT tracers were tested in two tumor models: orthotopic MDA231luc breast carcinoma (*8*) and spontaneous mouse lung carcinoma in bitransgenic mice (*11*). In both models, the tracers readily accumulated in the tumors (Figure 4A).

We further explored EGF-based ^{99m}Tc tracers by autoradiography of cryosections prepared from two MDA231luc tumor-bearing mice immediately after whole-body SPECT imaging. As shown in Figure 4B, radioactivity in tumors was significantly higher as compared with that from contralateral muscles. For autoradiography analysis of a spontaneous lung tumor, we selected a mouse with only a left lung tumor, as detected by SPECT with dEGF/Tc tracer. As shown in Figure 4C, autoradiography confirmed that radioactivity was significantly higher in left lung cryosections, as compared with that in the right lung.

PET Imaging. PET tracers were tested in orthotopic MDA231luc breast carcinoma. The tracers readily accumulated in large (10−15 mm) MDA231luc tumors, as imaged at 3 h

after tracer injection (Figure 5A). In separate experiments, we observed a selective uptake of EGF-based PET tracers in barely palpable MDA231luc tumors, whose presence was validated by bioluminescent imaging after intraperitoneal injection of luciferine (data not shown).

DISCUSSION

We describe here a family of EGF-based tracers for SPECT and PET imaging of EGF receptors. The tracers are based on natural monomeric and on engineered dimeric EGF, expressed with cysteine-containing Cys-tag for site-specific conjugation of various payloads (*10*). To obtain SPECT tracers, C4 in Cys-tag is directly radiolabeled with ^{99m}Tc, while PET tracers are prepared by site-specific conjugation of a PEGylated chelator DOTA to C4, followed by radiolabeling with ^{64}Cu. Both procedures avoid random conjugation of chelating moieties to targeting proteins, thus yielding uniform functionally active tracers with high specific activities. Importantly, direct radiolabeling with ^{99m}Tc yields a stable SPECT tracer with specific activity higher than that reported for the tracers based on EGF-chelator conjugates (*12, 13*). Rather similar tumor uptake is obtained with tracers based on monomeric and dimeric Cys-tagged EGF, although there are differences in biodistribution patterns that need to be further explored.

Over the years, several groups reported SPECT, PET, and fluorescent tracers for imaging EGF receptors, based on EGF (*8, 11, 13*−*21*), anti-EGFR antibodies (*21*−*27*), and low-molecular weight EGFR inhibitors (*28*−*33*). Since all of these tracers invariably imaged EGFR-positive tumors in mouse models, the eventual selection of the best candidate for further development would be based on relative advantages in terms of production, specific activity, biodistribution, and specific, receptor-mediated tumor uptake. Taking into account these criteria, we reasoned that using EGF, a natural EGFR ligand, as a targeting vector would be particularly advantageous. First, only functionally active and therefore critical for disease progression EGFRs will bind and internalize an EGF-based tracer. In contrast, tracers based on low-molecular weight kinase inhibitors or anti-EGFR antibodies would bind to all EGFRs, regardless of their functional status, providing, in this respect, information similar to that derived from immunohistochemistry. Second, continuous internalization of EGF-based tracers by recyclable EGFR would lead to intracellular accumulation of a radionuclide, thereby improving a signal-to-background ratio. Third, the small size of EGF, relative to that of antibodies, would facilitate tumor penetration with vastly better nonspecific soft tissue and blood clearance rates. Finally as a human protein, EGF is not expected to be immunogenic.

Although several EGF-based tracers have been described previously (*11, 13*−*21*), we expect that functionally active and uniform tracers based on Cys-tagged EGF would provide major advantages because they eliminate heterogeneity associated with random conjugation of contrast agents to the protein. Furthermore, comparison of biodistribution data for various EGF-based SPECT tracers suggests that our tracers provide a lower liver uptake and a similar or a lower kidney uptake (Table 1). Furthermore, kidney and liver uptake for our EGF-based SPECT tracers are in the range of those found for Annexin-HYNIC/^{99m}Tc tracer (*34*), which was approved for clinical trials (*35*). However, detailed preclinical dosimetry studies would be required for assessing the developmental potential of tracers based on Cys-tagged EGF or dEGF.

It should be noted that, similar to the other tracers based on physiologically active molecules, there are reasonable concerns of potential harmful pharmacological effects of EGF-based tracers. To begin addressing such concerns, we can compare the anticipated doses of EGF-based tracers with the dose of recombinant EGF used in a recent clinical trial. The tracer dose can be estimated based on the clinical experience with another protein-based SPECT tracer, annexin-HYNIC/Tc, that was injected at an average dose of 6.9 mCi per 77 kg patient or approximately 90 μCi/kg (*35*). Considering that EGF/Tc is readily labeled to a specific activity of 200 μCi/μg, a similar dose of EGF/Tc would require an injection of the tracer at a level of only 0.45 μg/kg. However, a recent clinical study of recombinant EGF for the treatment of neonatal necrotizing enterocolitis (*36*) concluded that a dose of 0.1 μg/hour/kg may be safely given via continuous infusion for 6 days, leading to a cumulative dose well above the anticipated EGF-tracer dose. Thus, although a definitive answer to safety concerns regarding EGF-based tracers requires extensive experimentation, we expect that injection of tracer amounts of EGF for diagnostic imaging will have no adverse effects.

LITERATURE CITED

(1) Baselga, J., and Arteaga, C. L. (2005) Critical update and emerging trends in epidermal growth factor receptor targeting in cancer. *J. Clin. Oncol. 23*, 2445–2459.

(2) Hann, C. L., and Brahmer, J. R. (2007) Who should receive epidermal growth factor receptor inhibitors for non-small cell lung cancer and when? *Curr. Treat. Opt. Oncol. 8*, 28–37.

(3) Bonomi, P. D., Buckingham, L., and Coon, J. (2007) Selecting patients for treatment with epidermal growth factor tyrosine kinase inhibitors. *Clin. Cancer Res. 13* (15 Pt 2), s4606–4612.

(4) Scagliotti, G. V., Selvaggi, G., Novello, S., and Hirsch, F. R. (2004) The biology of epidermal growth factor receptor in lung cancer. *Clin. Cancer Res. 10*, s4227–4232.

(5) Chung, K. Y., Shia, J., Kemeny, N. E., Shah, M., Schwartz, G. K., Tse, A., Hamilton, A., Pan, D., Schrag, D., Schwartz, L., Klimstra, D. S., Fridman, D., Kelsen, D. P., and Saltz, L. B. (2005 Cetuximab shows activity in colorectal cancer patients with tumors that do not express the epidermal growth factor receptor by immunohistochemistry. *J. Clin. Oncol. 23*, 1803–1810.

(6) Bell, D. W., Lynch, T. J., Haserlat, S. M., Harris, P. L., Okimoto, R. A., Brannigan, B. W., Sgroi, D. C., Muir, B., Riemenschneider, M. J., Iacona, R. B., Krebs, A. D., Johnson, D. H., Giaccone, G., Herbst, R. S., Manegold, C., Fukuoka, M., Kris, M. G., Baselga, J., Ochs, J. S., and Haber, D. A. (2005) Epidermal growth factor receptor mutations and gene amplification in non-small-cell lung cancer. Molecular analysis of the IDEAL/INTACT gefitinib trials. *J. Clin. Oncol. 23*, 8081–8092.

(7) Johns, T. G., Perera, R. M., Vernes, S. C., Vitali, A. A., Cao, D. X., Cavenee, W. K., Scott, A. M., and Furnari, F. B. (2007) The efficacy of epidermal growth factor receptor-specific antibodies against glioma xenografts is influenced by receptor levels, activation status, and heterodimerization. *Clin. Cancer. Res. 13*, 1911–1925.

(8) Backer, M. V., Levashova, Z., Patel, V., Jehning, B. T., Claffey, K., Blankenberg, F. G., and Backer, J. M. (2007) Molecular Imaging of VEGF receptors in angiogenic vasculature with single-chain VEGF based probes. *Nature Med. 13*, 509–514.

(9) Levashova, Z., Backer, M., Backer, J. M., and Blankenberg, F. G. (2008) Direct site-specific labeling of the Cys-tag moiety in scVEGF with Technetium 99m. *Bioconjugate Chem. 19*, 1049–1054.

(10) Backer, M. V., Levashova, Z., Levenson, R., Blankenberg, F. G., and Backer, J. M. (2008) Cysteine-Containing Fusion Tag for Site-Specific Conjugation of Therapeutic and Imaging Agents to Targeting Proteins. *Methods in Molecular Medicine. Volume 494: Peptide-Based Drug Design* (Otvos, L. Ed.) pp 275−294, Humana Press, New York.

(11) Hu, M., Scollard, D., Chan, C., Chen, P., Vallis, K., and Reilly, R. M. (2007) Effect of the EGFR density of breast cancer cells on nuclear importation, in vitro cytotoxicity, and tumor and normal-tissue uptake of [111In]DTPA-hEGF. *Nucl. Med. Biol. 34*, 887–896.

(12) Tran, T. P., Fan, A. C., Bendapudi, P. K., Koh, S., Komatsubara, K., Chen, J., Horng, G., Bellovin, D. I., Giuriato, S., Wang, C. S., Whitsett, J. A., and Felsher, D. W. (2008) Combined inactivation of MYC and K-Ras oncogenes reverses tumorigenesis in lung adenocarcinomas and lymphomas. *PLoS ONE 3*, e2125.

(13) Cornelissen, B., Kersemans, V., Burvenich, I., Oltenfreiter, R., Vanderheyden, J-L., Boerman, O., Vandewiele, C., and Slegers, G. (2005) Synthesis, biodistribution and effects of farnesyltransferase inhibitor therapy on tumour uptake in mice of 99mTc labelled epidermal growth factor. *Nucl. Med. Commun. 26*, 147–153.

(14) Babaei, M. H., Almqvist, Y., Orlova, A., Shafii, M., Kairemo, K., and Tolmachev, V. (2005) [99mTc]HYNIC-hEGF, a potential agent for imaging of EGF receptors in vivo: preparation and preclinical evaluation. *Oncol. Rep. 13*, 1169–1175.

(15) Capala, J., Barth, R. F., Bailey, M. Q., Fenstermaker, R. A., Marek, M. J., and Rhodes, B. A. (1997) Radiolabeling of epidermal growth factor with 99mTc and in vivo localization following intracerebral injection into normal and glioma-bearing rats. *Bioconjugate Chem. 8*, 289–925.

(16) Hnatowich, D. J., Qu, T., Chang, F., Ley, A. C., Ladner, R. C., and Rusckowski, M. Labeling peptides with technetium-99m using a bifunctional chelator of a N-hydroxysuccinimide ester of mercaptoacetyltriglycine. *J. Nucl. Med. 39*, 56–64.

(17) Ke, S., Wen, X., Gurfinkel, M., Charnsangavej, C., Wallace, S., Sevick-Muraca, E. M., and Li, C. (2003) Near-infrared optical imaging of epidermal growth factor receptor in breast cancer xenografts. *Cancer Res. 63*, 7870–7875.

(18) Adams, K. E., Ke, S., Kwon, S., Liang, F., Fan, Z., Lu, Y., Hirschi, K., Mawad, M. E., Barry, M. A., and Sevick-Muraca, E. M. (2007) Comparison of visible and near-infrared wavelength-excitable fluorescent dyes for molecular imaging of cancer. *J. Biomed. Optics. 12*, 024017.

(19) Kovar, J. L., Volcheck, W. M., Chen, J., and Simpson, M. A. (2007) Purification method directly influences effectiveness of an epidermal growth factor-coupled targeting agent for noninvasive tumor detection in mice. *Anal. Biochem. 361*, 47–54.

(20) Diagaradjane, P., Orenstein-Cardona, J. M., Colon-Casasnovas, N. E., Deorukhkar, A., Shentu, S., Kuno, N., Schwartz, D. L., Gelovani, J. G., and Krishnan, S. (2008) Imaging epidermal growth factor receptor expression in vivo: pharmacokinetic and biodistribution characterization of a bioconjugated quantum dot nanoprobe. *Clin. Cancer Res. 14*, 731–741.

(21) Reilly, R. M., Kiarash, R., Sandhu, J., Lee, Y. W., Cameron, R. G., Hendler, A., Vallis, K., and Gariepy, J. (2000) A comparison of EGF and MAb 528 labeled with 111In for imaging human breast cancer. *J. Nucl. Med. 41*, 903–911.

(22) Rosenthal, E. L., Kulbersh, B. D., Duncan, R. D., Zhang, W., Magnuson, J. S., Carroll, W. R., and Zinn, K. (2006) In vivo detection of head and neck cancer orthotopic xenografts by immunofluorescence. *Laryngoscope 116*, 1636–1641.

(23) Rahman, M., Abd-El-Barr, M., Mack, V., Tkaczyk, T., Sokolov, K., Richards-Kortum, R., and Descour, M. (2005) Optical imaging of cervical pre-cancers with structured illumination: an integrated approach. *Gyn. Oncol. 99* (3, Suppl 1), S112–S115.

(24) Dadparvar, S., Krishna, L., Miyamoto, C., Brady, L. W., Brown, S. J., Bender, H., Slizofski, W. J., Eshleman, J., Chevres, A., and Woo, D. V. (1994) Indium-111-labeled anti-EGFr-425 scintigraphy in the detection of malignant gliomas. *Cancer. 73*, 884–889.

(25) Vallis, K. A., Reilly, R. M., Chen, P., Oza, A., Hendler, A., Cameron, R., Hershkop, M., Iznaga-Escobar, N., Ramos-Suzarte, M., and Keane, P. (2002) A phase I study of 99mTc-hR3 (DiaCIM), a humanized immunoconjugate directed towards the epidermal growth factor receptor. *Nucl. Med. Commun. 23*, 1155–1164.

(26) Schechter, N. R., Yang, D. J., Azhdarinia, A., Kohanim, S., III., Oh, C. S., Hu, M., Yu, D. F., Bryant, J., Ang, K. K., Forster, K. M., Kim, E. E., and Podoloff, D. A. (2003) Assessment of epidermal growth factor receptor with 99mTc-ethylenedicysteine-C225 monoclonal antibody. *Anti-Cancer Drugs 14*, 49–56.

(27) Hsu, E. R., Anslyn, E. V., Dharmawardhane, S., Alizadeh-Naderi, R., Aaron, J. S., Sokolov, K. V., El-Naggar, A. K., Gillenwater, A. M., and Richards-Kortum, R. R. (2004) A far-red fluorescent contrast agent to image epidermal growth factor receptor expression. *Photochem. Photobiol. 79*, 272–279.

(28) Mishani, E., Abourbeh, G., Rozen, Y., Jacobson, O., Laky, D., Ben David, I., Levitzki, A., and Shaul, M. (2004) Novel carbon-11 labeled 4-dimethylamino-but-2-enoic acid [4-(phenylamino)-quinazoline-6-yl]-amides: potential PET bioprobes for molecular imaging of EGFR-positive tumors. *Nucl. Med. Biol. 31*, 469–476.

(29) Shaul, M., Abourbeh, G., Jacobson, O., Rozen, Y., Laky, D., Levitzki, A., and Mishani, E. (2004) Novel iodine-124 labeled EGFR inhibitors as potential PET agents for molecular imaging in cancer. *Bioorg. Med. Chem. 12*, 3421–3429.

(30) Mishani, E., Abourbeh, G., Jacobson, O., Dissoki, S., Ben Daniel, R., Rozen, Y., Shaul, M., and Levitzki, A. (2005) High-affinity epidermal growth factor receptor (EGFR) irreversible inhibitors with diminished chemical reactivities as positron emission tomography (PET)-imaging agent candidates of EGFR overexpressing tumors. *J. Med. Chem. 48*, 5337–5348.

(31) Bonasera, T. A., Ortu, G., Rozen, Y., Krais, R., Freedman, N. M., Chisin, R., Gazit, A., Levitzki, A., and Mishani, E. (2001) (18)F-labeled biomarkers for epidermal growth factor receptor tyrosine kinase. *Nucl. Med. Biol. 28*, 359–374.

(32) Wang, J. Q., Gao, M., Miller, K. D., Sledge, G. W., and Zheng, Q. H. (2006) Synthesis of [11C]Iressa as a new potential PET cancer imaging agent for epidermal growth factor receptor tyrosine kinase. *Bioorg. Med. Chem. Lett. 16*, 4102–416.

(33) Gelovani, J. G. (2008) Molecular imaging of epidermal growth factor receptor expression-activity at the kinase level in tumors with positron emission tomography. *Cancer Metast. Rev. 27*, 645–653.

(34) Fonge, H., de Saint, H. M., Vunckx, K., Rattat, D., Nuyts, J., Bormans, G., Ni, Y., Reutelingsperger, C., and Verbruggen, A. (2008) Preliminary in vivo evaluation of a novel 99mTc-labeled HYNIC-cys-annexin A5 as an apoptosis imaging agent. *Bioorg. Med. Chem. Lett. 18*, 3794–3798.

(35) Kemerink, G. J., Liu, X., Kieffer, D., Ceyssens, S., Mortelmans, L., Verbruggen, A. M., Steinmetz, N. D., Vanderheyden, J. -L., Green, A. M., and Verbeke, K. (2003) Safety, biodistribution, and dosimetry of 99mTc-HYNIC-annexin V, a novel human recombinant annexin V for human application. *J. Nucl. Med. 44*, 947–952.

(36) Sullivan, P. B., Lewindon, P. J., Cheng, C., Lenehan, P. F., Kuo, B. S., Haskins, J. R., Goodlad, R. A., Wright, N. A., and de la Iglesia, F. A. (2007) Intestinal mucosa remodeling by recombinant human epidermal growth factor (1−48) in neonates with severe necrotizing enterocolitis. *J. Pediatr. Surg. 42*, 462–469.

BC800443W